RESEARCH

Experimental and Numerical Assessments of Slab-Column Connections Strengthened Using Bonded Hemp Fiber Fabric Sheets

Loai Khaled Al-Mawed and Bilal Salim Hamad[*]

Abstract

The replacement of synthetic fibers with natural fibers in concrete has been recently investigated to counter the growing environmental and sustainable issues. Hemp fibers are environmentally friendly and are used in the manufacturing of composite materials. This paper reports on the experimental assessment of using hemp fiber reinforced polymer (HFRP) fabric sheets as an alternative to carbon fiber reinforced polymer (CFRP) sheets to strengthen interior slab-column connections. Small-scale interior slab-column connections were loaded centrally through the column stub up to failure. The main test variables were slab thickness, HFRP sheet width, number of HFRP layers, type of strengthening material (HFRP or CFRP sheets), and HFRP sheet's location relative to the column's face. Assessment of the strengthening material was based on a comparison of load capacity, mode of failure, load–displacement history, and cracking patterns. The experimental results demonstrated that HFRP strengthening sheets led to improvement in the structural behavior of the slab-column connections depending on the slab thickness, width and configuration for HFRP sheets. Although the HFRP sheets led to lower improvement as compared to the synthetic CFRP sheets, however, the same improvement could be reached by the HFRP sheets if they are applied in larger width or different configurations. A finite-element model was developed using ABAQUS software to predict the behavior of simulated specimens. The numerical findings showed that the models predicted the connection behavior in good agreement with the experimental test results. In addition, an analytical model was calibrated to simulate the behavior of the tested specimens.

Keywords: concrete connection, natural fibers, HFRP, synthetic fibers, CFRP, punching shear strengthening, concrete damaged plasticity (CDP), ABAQUS

1 Introduction

Evaluation indicators of civil engineering projects include serviceability, strength, durability, and cost. In most cases, the main concerns in building structures are having good performance and minimizing cost, while minor considerations are given to sustainability and environmental impact. Many buildings nowadays are constructed using a flat reinforced concrete (RC) slab system composed of flat slab supported on columns without beams. The advantages of using a flat plate system include faster construction, reducing floor-to-floor height, and more economical construction compared to other structural systems. However, in the flat slab, the connection between the column and the slab is most critical because of its susceptibility to punching shear failure which is a brittle and non-ductile failure that has caused the collapse of many structures in the last century (King & Delatte, 2004; Mirzaei & Sasani, 2011).

Punching shear strength of flat slabs can be inadequate due to changing the building's use, increasing the floor

*Correspondence: bhamad@aub.edu.lb

CEE Department, American University of Beirut, PO Box 11-0236, Riad El-Solh, Beirut, Lebanon

loading, installing a new slab opening in the column's vicinity, corrosion of the reinforcement, or design construction errors. In these situations, the slab must be replaced or strengthened. Strengthening could be more cost-effective than the replacement of the slab. Existing methods for improving the punching shear capacity in flat plates include section enlargement (providing drop panel or column capital around the column) or adding additional steel components (installing shear bolts or a combination of steel plates and transverse pre-stressed steel bolts around the column). However, these methods are expensive and disturb the usage of the building.

2 Literature Review

2.1 Recent Research on Strengthening of Interior Slab-Column Connections Using Synthetic Sheets

In the past two decades, several studies have investigated the effectiveness of using CFRP sheets and Glass Fiber-Reinforced Polymer (GFRP) laminates as strengthening techniques for slab column connections, such as those reported by (Chen & Chen, 2020; Chen & Li, 2005; Harajli & Soudki, 2003; Harajli et al., 2006; Sharaf et al., 2006; Soudki et al., 2012).

Harajli and Soudki (2003) investigated the enhancement in punching shear strength of interior slab-column connections using externally bonded CFRP sheets. They tested sixteen small-scale interior connections, each consisting of a 670×670 mm square slab with a 100×100 mm center column stub. The test parameters included the thickness of the slab (55 or 75 mm), the ratio of steel reinforcement (1 or 1.5%), and the area of the CFRP sheets. Each specimen was supported over the four edges and subjected to point load through the column until failure. Test results showed that externally bonded CFRP sheets considerably enhanced the flexural and shear capacities of the specimen but reduced the ductility of the mode of failure. The capacity enhancement varied based on the investigated test parameters and changed the failure mode of the connection from pure flexural to a combined flexural–shear mode or pure punching mode.

Moreover, Chen and Li (2005) investigated the use of GFRP Laminates as strengthening material for interior concrete slab-column connections to improve the punching shear capacity. They tested eighteen specimens, each consisting of a $1000 \times 1000 \times 100$ mm square slab with a 150×150 mm square column extending 150 mm from the top of the slab surface. The test parameters included concrete compressive strength (14 or 28 MPa), tension steel reinforcement ratio (0.59% or 1.31%), and the number of GFRP laminate layers (one or two layers). Test results indicated that GFRP laminates markedly enhanced the ultimate punching shear capacity for interior slab-column connections. This enhancement was influenced by the test variables described above and was more effective for slabs with the lower compressive strength and reinforcement ratio. It was also concluded that using GFRP laminates could change the mode of failure of the connection from flexural failure to punching shear failure.

Chen and Chen (2020) tested twelve slab-column specimens. The slab was $1000 \times 1000 \times 100$ mm and the column was 150×150 mm. Test variables included the concrete compression strength f'c (14 or 28 MPa), the tensile steel reinforcement ratio (0.6 or 1.2%), and the number of layers of CFRP laminates (one or two layers). The concrete slab was simply supported along the four edges. The specimen was subjected to a concentrated load through the column's stub and was loaded until failure. Test results indicated that externally bonded CFRP laminates significantly improved the punching shear strength of the tested connections, especially specimens with the lower reinforcement ratio.

2.2 Recent Research on Strengthening Beams and Columns Using HFRP Sheets

Strengthening concrete elements using natural fibers instead of synthetic fibers has many environmental benefits including carbon neutrality, reducing the consumption of non-degradable polyethylene that leads to serious environmental problems, and the fact that natural fibers are renewable materials. As a result, the replacement of synthetic fibers by natural fibers will lead to sustainable development. Awwad et al. (2014) reported on the positive effect of hemp fibers added to the concrete mix on the ductility of the load–deflection history of reinforced concrete members.

However, it should be noted that the primary deficiency of hemp fibers is the uncertainty of the physical and mechanical properties due to its composition variability. Many factors may influence the variability in diameters and properties of natural fibers including source, age, geographic origin and rainfall during growth (Rahman Khan et al., 2011).

Yinh et al. (2016) investigated the applicability of using natural hemp fiber fabric sheets as strengthening material. They tested five full-scale reinforced concrete beams to study the efficiency of using sheets of epoxy bonded HFRP composites for flexural strengthening of RC beams. Test variables included fiber sheet thickness (one or two layers) and strengthening configuration (tension side only or U-wrap). Test results showed that HFRP sheets significantly increased the flexural strength and stiffness of the tested beams. Increasing the thickness of the HFRP sheets led to an increase in flexural strength. In addition, the U-wrapping strengthening scheme was more efficient than the tension side one.

Ghalieh et al. (2017) studied the efficiency of HFRP sheets as external confinement for concrete columns. Axial compression test was performed on 30 concrete cylinders. The main test variables included the number of confining layers (1, 2, or 4 layers) and the column slenderness (length to diameter) ratio (1.5, 2, 2.5, or 3). Test results indicated that HFRP sheets improved the reinforced concrete column's axial compressive strength and ductility. The improvement increased as the number of hemp fiber sheets increased but decreased with the increase of slenderness ratio.

Furthermore, Siriluk et al. (2018) examined the effectiveness of HFRP sheets in enhancing the shear strength of reinforced concrete deep beams. HFRP sheets were bonded to the exterior surface of the beams using epoxy resin. All beams were tested under three-point loading; the load was applied at mid-span. Test parameters included the number of HFRP sheet layers (1 or 2) and the strengthening configuration (both-side bonded sheets or three-side bonded U-shape sheets). Experimental results revealed that HFRP sheets improved the ultimate shear load and deflection capacity of the tested beams. The shear strength increased upon doubling the number of strengthening sheets, and the U-shape strengthening configuration was more effective than both side one.

2.3 Recent Research Using Concrete Damaged Plasticity (CDP) Model to Simulate Slab-Column Connections

Lubliner et al. (1989) introduced and verified a constitutive model for non-linear analysis of concrete, based on an internal variable-formulation of plasticity theory. This model was adopted later by the finite-element software ABAQUS under the name of concrete damage plasticity (CDP). This model was later subjected to some modifications by Lee and Fenves (1998). CDP is a continuum, plasticity-based, damage model for concrete behavior. It is governed by two main failure mechanisms of the concrete material: tensile cracking and compressive crushing. Several research studies used CDP to simulate reinforced concrete slab-column connections.

Genikomsou and Polak (2016) simulated four interior reinforced concrete slab-column connections reinforced with different amounts of shear bolts using the damaged plasticity model in ABAQUS. Comparison of the values of the failure loads was conducted between design codes, numerical findings, and experimental results. Genikomsou and Polak concluded that that the numerically predicted load–deflection responses and cracking propagation of the simulated connections were closely aligned with the experimental results.

Silva et al. (2019) conducted experimental and numerical studies to examine the effect of externally bonded CFRP sheets on the punching shear capacity of interior slab-column connections. Four different strengthening schemes were tested. Silva et al. used the ABAQUS package to simulate the experimental program using the CDP model. The numerical results showed that the model predicted the structural behavior of the connections in good agreement with the experimental test results.

3 Research Significance and Scope

The literature review has revealed that strengthening interior slab-column connections using synthetic fibers (externally bonded CFRP or GFRP sheets) would increase the shear capacity of the connection. Other reported studies have shown improvement in the compression capacity of columns as well as the flexural and shear capacities of beams strengthened by HFRP fabric sheets. However, there is limited knowledge on the effectiveness of using natural HFRP fabric sheets in increasing the punching shear capacity of the concrete connections. The main objective of this study is to examine the viability of using HFRP fabric sheets as an alternative to CFRP sheets for punching shear strengthening of reinforced concrete slab-column connections. This study was conducted at the Material Laboratory of the American University of Beirut (AUB). Analysis of the test results was performed in terms of the mode of failure, the ultimate shear capacity, and the load–deflection response of the tested specimens. A numerical model was calibrated to simulate the behavior of tested specimens, and an analytical model was adopted from the literature to predict the punching shear capacity of the tested specimens.

4 Experimental Test Program

It is important to note that the size and fabrication of the test specimen, the strengthening configuration, sheets installation, and the test or load setup were all similar to what was used in previous research studies reported in the literature on evaluation of shear strengthening of slab column connections using externally bonded CFRP sheets (Harajli & Soudki, 2003; Harajli et al., 2006; Soudki et al., 2012). Absolute values of the test results of the different specimens were not the objective of the study. What was important was the effect of the various variables on the comparative performance of the HFRP strengthened specimens on one hand and the CFRP strengthened specimens and the control un-strengthened specimens on the other hand.

4.1 Test Specimens and Parameters

Eleven small-scale interior reinforced concrete 670×670 mm slab-column specimens, each with a 100×100 mm center column stub extending 150 mm from the slab's top surface and 50 mm from the bottom

surface, were tested using the MTS Universal Testing Machine. The geometry of the specimens takes into consideration the machine's opening limitations. Fig. 1 shows the typical specimen dimensions. The details of the specimens were chosen to be similar to those used by Harajli and Soudki (2003) who investigated the enhancement in

punching shear strength of interior slab-column connections using externally bonded CFRP sheets.

The main test variables were the slab thickness (55 or 75 mm), width of hemp fiber fabric sheet (150 or 200 mm), number of layers of HFRP sheets (one or two layers), and location of the hemp strips (adjacent to the column or offset by 1.5d from the face of the column). The chosen slab thickness values (55 and 75 mm) correspond to span-to-depth ratios of 25 and 18, respectively, assuming the supports to be lines of contra flexure. To make a comparison between the effect of HFRP sheets and CFRP sheets, two of the 11 specimens were strengthened by 150 mm wide CFRP sheets. Fig. 2 shows the used strengthening schemes.

It should be noted that the slab thicknesses were selected in this study to assess the performance of HFRP in connections with high and relatively low flexural capacity. The size and the configuration of strengthening strips used in this investigation were chosen to give a fair improvement in the overall structural behavior of the connections. The double layers parameter was studied to examine whether adding more layers of the HFRP sheet would affect the behavior of the strengthened connection or not.

The 11 specimens are divided into two groups, SA and SB, based on slab thicknesses: 55 for SA and 75 mm for SB. Test variables are listed in Table 1. Each specimen is identified by a three-part notation system. The first part is SA or SB. The second part refers to the type of
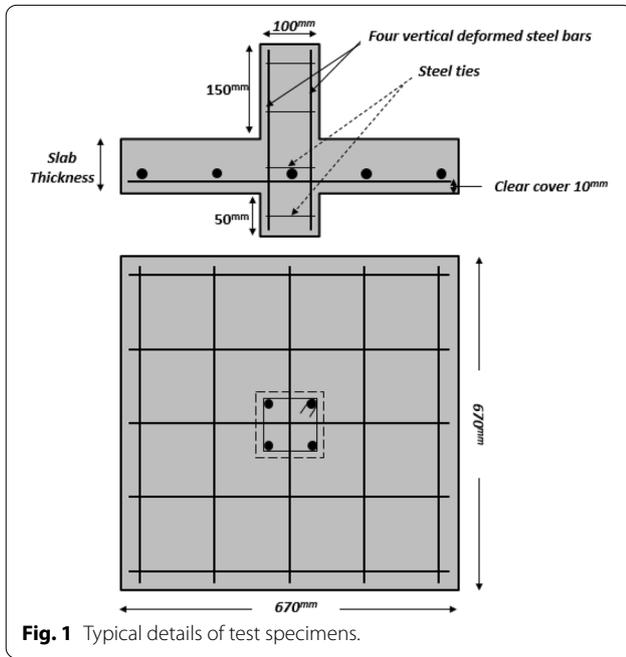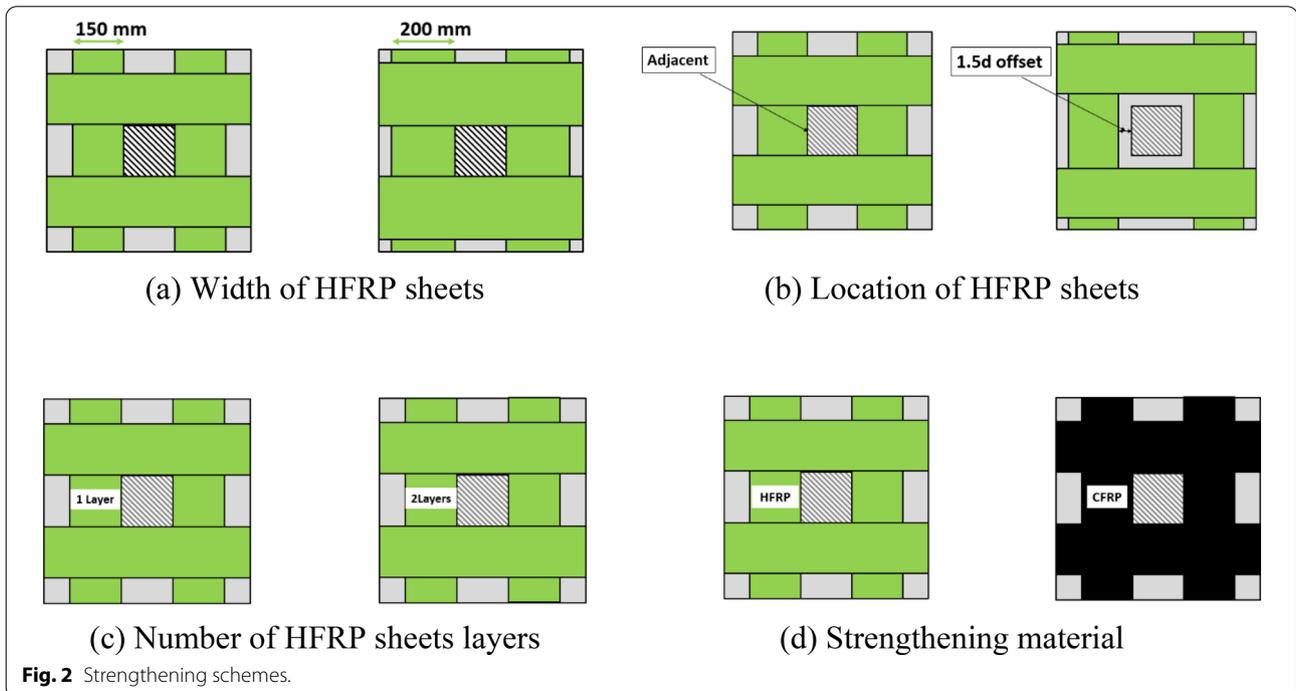

Fig. 1 Typical details of test specimens.

(a) Width of HFRP sheets

(b) Location of HFRP sheets

(c) Number of HFRP sheets layers

(d) Strengthening material

Fig. 2 Strengthening schemes.

Table 1 Summary of test variables.

Group	Specimen designation	Slab Thickness (mm)	Steel ratio (%)	FRP type	FRP width (cm)	No. of layers	Strengthening configuration
SA	SA0	55	1	–	–	–	–
	SA-H15-A	55	1	HFRP	15 cm	1	Adjacent
	SA-H15-O	55	1	HFRP	15 cm	1	Offset
	SA-H20-A	55	1	HFRP	20 cm	1	Adjacent
	SA-C15-A	55	1	CFRP	15 cm	1	Adjacent
SB	SB0	75	1	–	–	–	–
	SB-H15-A	75	1	HFRP	15 cm	1	Adjacent
	SB-H15-O	75	1	HFRP	15 cm	1	Offset
	SB-H20-A	75	1	HFRP	20 cm	1	Adjacent
	SB-H15(2)-A	75	1	HFRP	15 cm	2	Adjacent
	SB-C15-A	75	1	CFRP	15 cm	1	Adjacent

strengthening sheet (H for hemp fabric and C for CFRP) and the strengthening sheet's width (15 or 20 cm). The number in parenthesis, if it exists, implies two layers of strengthening sheets. The third part of the notation refers to the location of the HFRP fabric strips relative to the column side: A for adjacent and O for offset by 1.5d from the column's face. SA0 and SB0 are the control un-strengthened specimens in groups SA and SB, respectively.

4.2 Testing Materials
4.2.1 Concrete
Normal weight concrete was used throughout the experimental program. The concrete mix consisted of Portland cement Type I, sand, and well-graded crushed limestone aggregates with a maximum size of 10 mm. The intended concrete compressive strength for all specimens was 35 MPa. The batching weights in kg per cubic meter of concrete were 485 (cement), 1265 (coarse aggregates), 630 (sand), and 242.5 (water). The water–cement ratio was 0.5. A su2019perplasticizer dosage of 0.4% by weight of cement was added to increase the concrete mix's consistency. The superplasticizer conformed to ASTM C494 (2019). The actual concrete compression strength of each mix was determined by testing 150×300 mm standard cylinders according to ASTM C39, (2021). The specimens were cast using a small mixer in the lab, and the specimens and their corresponding cylinders were cured for 28 days before testing.

4.2.2 Reinforcing Steel
All specimens in Group SA of 55 mm thick slabs were reinforced using five 8 mm Grade 60 deformed bars in each direction (1% reinforcement ratio). On the other hand, the reinforcement in Group SB of 75 mm thick specimens consisted of five 10 mm Grade 60 deformed bars in each direction (1% reinforcement ratio). Using a clear concrete cover of 10 mm, the average effective depth (d) to the two reinforcement layers' centers was 37 mm for the SA specimens and 55 mm for the SB specimens. Four deformed vertical bars were placed at the column stub's corners, 8 mm in diameter for the SA specimens and 10 mm for the SB specimens. The four-column bars were tied together by four ties spaced at 78 mm. Typical dimensions and steel reinforcement layout of the test specimens are shown in Fig. 1. Two coupons of the 8 mm and 10 mm bars were tested, and the yield and ultimate strength values were 570 and 640 MPa, respectively.

4.2.3 HFRP Fabric Sheet
Hemp Traders supplied the hemp fabric sheets utilized in this study under the product name "CS-C11-DRK". The tensile properties of the bi-directional HFRP fabric sheets used were determined by performing a tensile test of three HFEP strips according to ASTM D3822/D3822M-14 (2020). The three 25×300 mm strips were impregnated in epoxy resin and left to dry. After removing excess epoxy, the average thickness of the strips was 1.2 mm. The strips were extended at a constant rate of 1 mm/min, and when a stress of 30 MPa was reached, the strips exhibited a sudden brittle failure. The modulus of elasticity is 3.7 GPa and the ultimate strain is 0.035 mm/mm.

4.2.4 CFRP Sheet
The CFRP strengthening sheets used in four out of the 24 specimens are SikaWrap®-230 C (2017). The mechanical properties of the CFRP sheets, as supplied by the manufacturer, are shown in Table 2.

Table 2 Properties of the CFRP SikaWrap-230 C.

CFRP Strips (SikaWrap-230 C)	
Width (mm)	1000
Thickness (mm)	0.129
Modulus of elasticity (GPa)	230
Tensile strength (MPa)	3,500
Elongation at break (%)	1.59
Apparent density (g/cm^3)	1.82

4.2.5 The Adhesive Sikadur-330

The adhesive used to bond the strengthening material (HFRP or CFRP sheets) to the test specimens was Sikadur®-330 (2019). It is a two-component, thixotropic epoxy-based impregnating resin, where the mix ratio of Component A to Component B by weight is 4 to 1. The mechanical properties of the epoxy Sikadur-330 as provided by the supplier are given in Table 3.

4.2.6 Strengthening Procedure

The HFRP fabric sheets were cut into the desired length and width for strengthening the concrete slab. The sheet installation procedure started by removing all the dust and impurities on the slab-column specimen's tension side using abrasive sheets and a vacuum machine. A thin layer of epoxy was applied at the proper location then a saturated strengthening sheet with epoxy resin was laid above the epoxy layer. A rubber roller was passed on the installed fabric sheet to make sure no air bubbles were trapped between the fabric, the epoxy layer, and the concrete surface. Fig. 3 shows a test specimen after installing the hemp fabric sheets.

4.3 Test Setup

The load was applied on the specimen through the column stub and was increased monotonically until failure (refer to Fig. 4). The test was displacement controlled, where the load was applied at an approximate average rate of 1 mm/min. The specimens were mounted on a steel frame with 40 mm wide pedestals on all four sides; the corners of the slab were free to lift when the

Table 3 Mechanical properties of the epoxy Sikadur-330

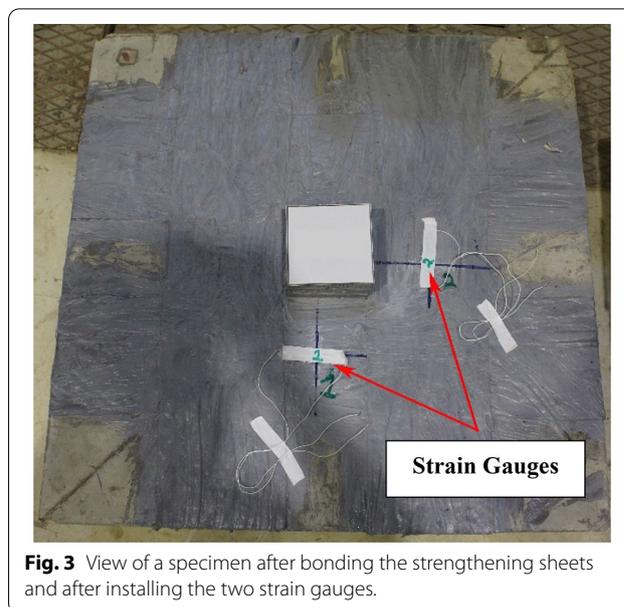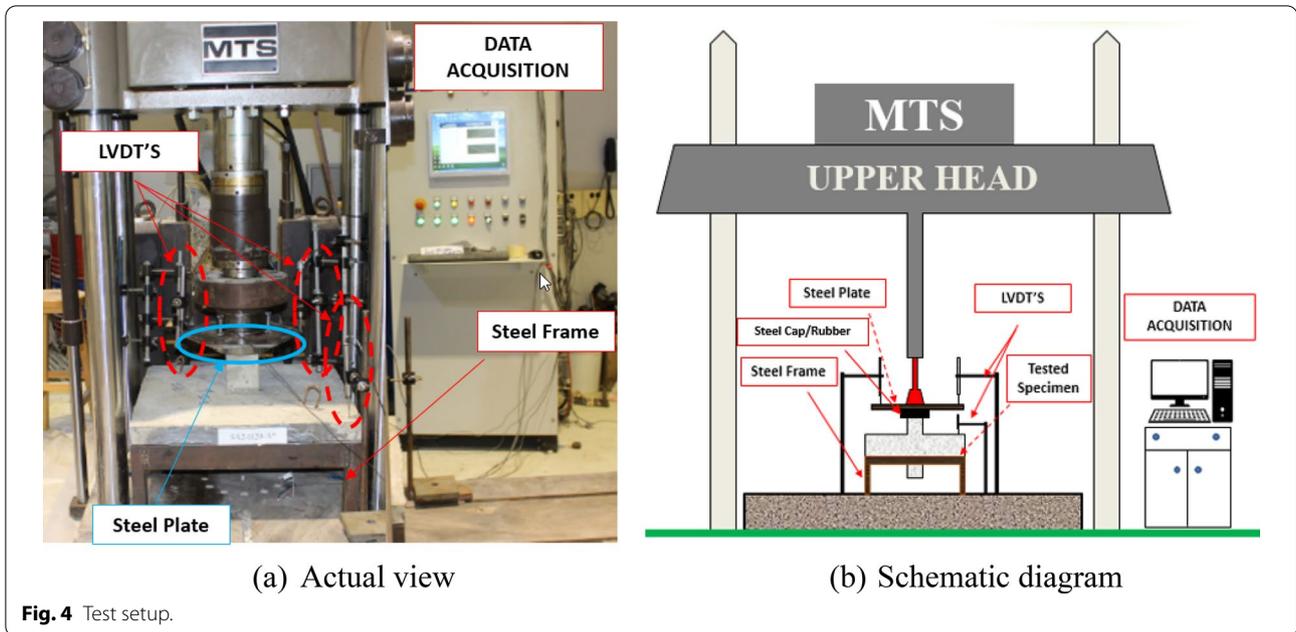| Adhesive Paste (Sikadur-330)	
Density (Kg/L)	1.3
Tensile strength at 7 days (MPa)	30
Elongation at break at 7 days (%)	0.9
Modulus of elasticity at 7 days (MPa)	4,500
Flexural Modulus at 7 days (MPa)	3,800

Fig. 3 View of a specimen after bonding the strengthening sheets and after installing the two strain gauges.

load was applied. A steel cap with a rubber heading was placed on the column stub's top to distribute the load monolithically so that the column would not fail before the slab. Test measurements included the applied load, slab deflection at the column location, and the strain in the HFRP or CFRP strips. Two linear variable differential transformers (LVDT's) were placed on steel plates on opposite sides of the tested specimen. The LVDT's deflection readings were averaged to obtain the displacement at the center of the slab. A third LVDT was placed on one of the slab specimens' corners to detect the uplifting value during testing. Two strain gauges were installed, one at mid-length of each of two perpendicular strengthening strips, to measure the strain in the HFRP or CFRP strips, as shown in Fig. 3. The readings of the applied load, the LVDT's, and strain gauges were monitored by a data acquisition system.

4.4 Preliminary Trial Tests

Prior to launching the full experimental program, a pilot study was conducted on several specimens with replicates to check the applicability of using HFRP fabric sheets to strengthen interior slab column connections, to decide on the variables to consider in the research program, to check the viability of using epoxy sikadur-330 to bond the HFRP fabric sheets on the slab's tension side which is the same epoxy type recommended for bonding CFRP sheets, and to check the reliability of the test setup and the test results. The promising results of the preliminary study made possible the initiation of the full experimental program.
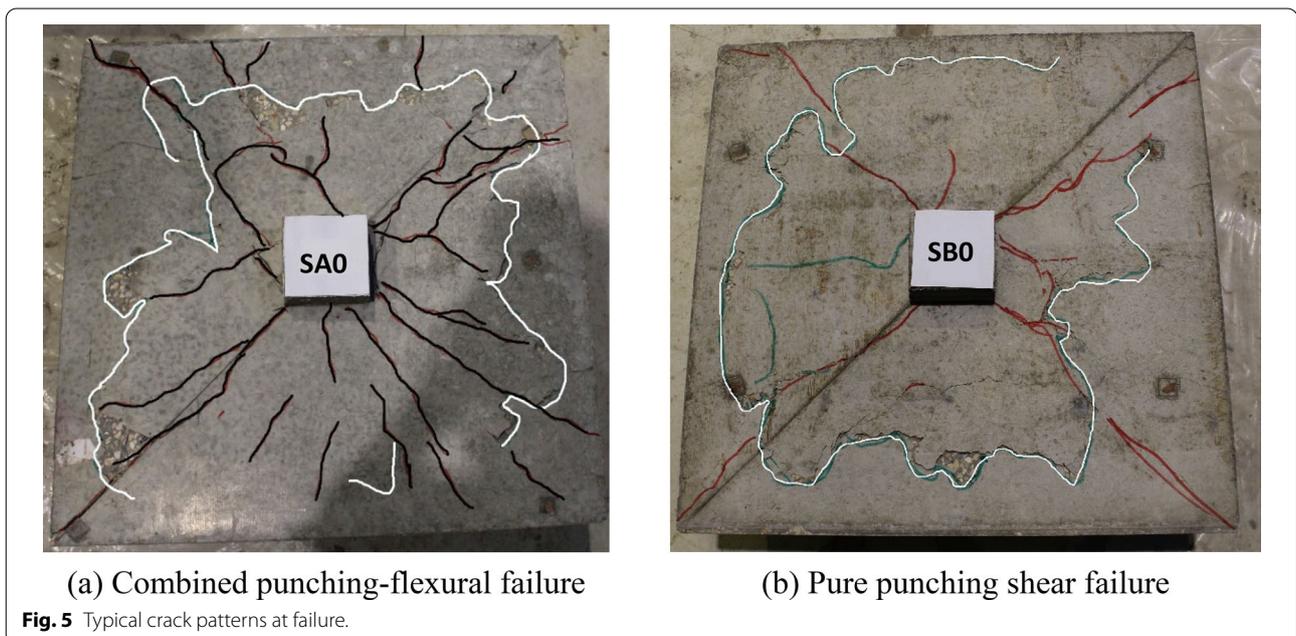
(a) Actual view

(b) Schematic diagram

Fig. 4 Test setup.

5 Experimental Test Results

5.1 Failure Modes

Two modes of failure were noticed: pure punching shear failure and combined punching-flexural failure. All specimens showed clear evidence of brittle punching shear failure except the three specimens of Group SA: SA0, SA-H20-A, and SA-C15-A, which experienced a more ductile mode of failure. Mirrors were used during the 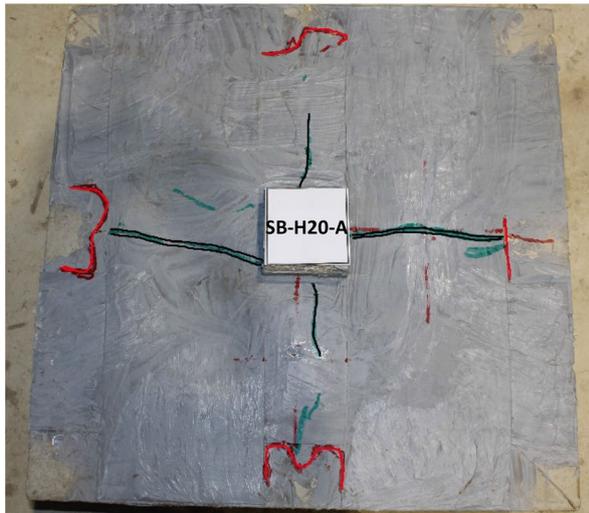testing procedure to monitor the tension side cracking pattern and mode of failure of control specimens. The ductile mode of failure of SA0 started with flexural yield lines at the corners of the column which propagated later towards the edges of the slab, followed by punching shear cracks that were characterized by one major circumferential crack (refer to Fig. 5a). Observation after failure of the tension side of the SA-H20-A, and SA-C15-A, indicated similar cracking patterns as SA0. Failure of the control specimen SB0 was

(a) Combined punching-flexural failure

(b) Pure punching shear failure
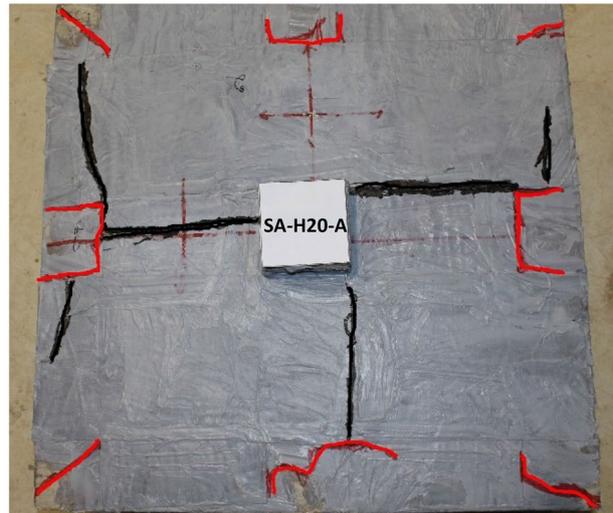
Fig. 5 Typical crack patterns at failure.

detected by observing inclined cracks forming at a distance away from the column stub's perimeter in the slab tension face, as shown in Fig. 5b, followed by sudden and noisy punching of the column through the slab, similar observations were made for the remaining two specimens in Group SA and all six specimens of Group SB.

Failure of most specimens strengthened by HFRP sheets was preceded by tearing or breaking of the HFRP sheets in the critical maximum moment region (at mid-length of the HFRP sheets), and bond failure between the HFRP sheets and the concrete surface was found along the major cracks of the specimens, as shown in Fig. 6a. Failure of specimen SA-H20-A was accompanied by breaking of HFRP sheets not only in its mid-length but also two of the sheets broke near the supports (see Fig. 6b).

(a) Failure of specimen SB-H15-O   (b) Failure of specimen SA-H20-A

Fig. 6 Failure of specimens confined and strengthened by HFRP sheets.

(a) Failure of specimen SA-C15-A   (b) Debonding of CFRP sheets in SA-C15-A

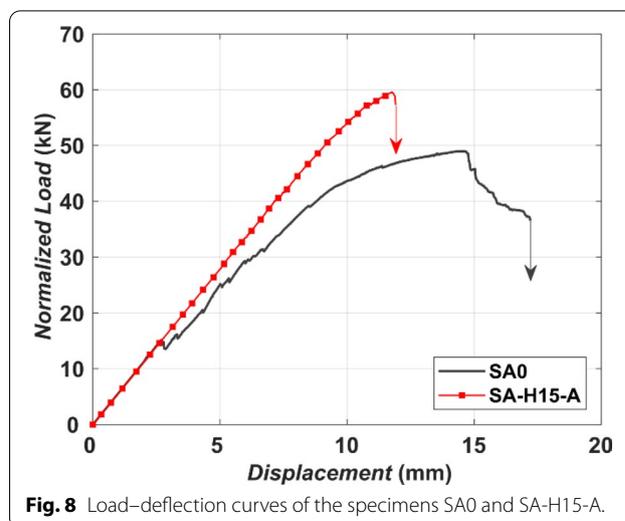**Fig. 7** Failure of specimens confined and strengthened by CFRP sheets.

On the other hand, the CFRP strengthened specimens did not show a break or fracture of the CFRP sheets. However, due to the fact that CFRP sheets have no resistance in the transverse direction, a detachment of these sheets was observed on either side of the punching shear cracks plane, as shown in Fig. 7a. A delamination failure of CFRP sheets was observed in specimen SA-C15-A, where the whole CFRP sheets system could be effortlessly removed from the slab surface after the specimen's failure occurred (refer to Fig. 7b).

5.2 Presentation and Analysis of Test Results

Test results of all 11 specimens are presented in Table 4. The results include $f'c$ at the day of testing; the ultimate load normalized at a common $f'c$ of 35 MPa by multiplying the actual experimental value by $\sqrt{f'c/35}$, percentage change of the ultimate load relative to the control specimen in the group, deflection at ultimate load, fracture energy calculated as the area under the load–deflection curve, energy ductility index computed as the fracture energy of the specimen divided by the fracture energy of the control specimen in the same group, the initial stiffness or slope of the load–deflection curve, and the percentage change in the initial stiffness relative to the control specimen in the same group.

5.2.1 Load–Deflection Response

Fig. 8 shows a comparison between the normalized load versus deflection curve of two specimens, one that failed in pure punching shear failure (SA-H15-A) and another one that failed in combined punching-flexural failure (SA0). Apparently, the shape of load–deflection curves can be used to distinguish the failure type of the

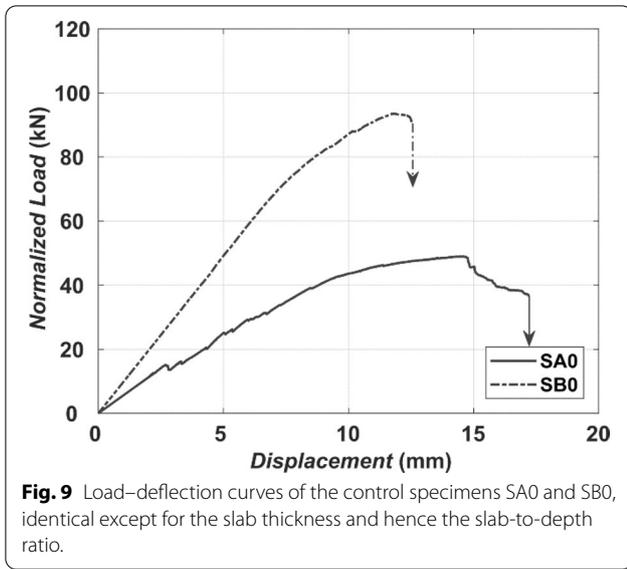**Fig. 8** Load–deflection curves of the specimens SA0 and SA-H15-A.

specimens. All specimens displayed an almost bilinear behavior up to the ultimate load that can be divided into two phases: the first phase of response is characterized by the initial stiffness of the un-cracked slab at the early loading stage, and the second phase can be identified by a reduction in the stiffness due to the development of tensile flexural cracks. After the ultimate load is reached, the specimen that experienced pure punching shear failure had a very sharp drop in load. The other specimen that had combined punching flexural failure experienced relatively more considerable deflections in the post-ultimate stage due to the reinforcing bars' yielding before the occurrence of the punching shear failure, which resulted in a sharp drop of the load.

Table 4 Summary of the test results.

Group	Specimen Designation	f(MPa)	Normalized ultimate load P_U (kN)	Ratio of ultimate loads (%)	Deflection at ultimate load (mm)	Fracture energy (kN-m)	Energy Ductility Index	Initial stiffness (kN/mm)	Stiffness Increase (%)
SA	SA0*	43.7	49	-	14.58	0.563	-	4.6	-
	SA-H15-A	36.5	59.6	21.63%	11.763	0.3935	0.7	5.58	20.9%
	SA-H15-O	36.5	62.94	28.44%	11.84	0.4466	0.79	6.32	37.03%
	SA-H20-A*	32.4	69.16	41.14%	13.15	0.752	1.34	7.232	56.8%
	SA-C15-A*	38.3	69.7	42.24%	10.94	0.813	1.44	7.14	54.8%
SB	SB0	33.6	93.57	-	11.77	0.711	-	9.81	-
	SB-H15-A	36.5	98.9	5.7%	10.09	0.566	0.796	10.742	9.5%
	SB-H15-O	30	108.25	15.7%	11.6	0.729	1.03	11.324	15.4%
	SB-H20-A	36.5	100.35	7.25%	10.16	0.597	0.84	11.7	19.25%
	SB-H15(2)-A	35	102.43	9.47%	11.32	0.6972	0.98	11.48	17%
	SB-C15-A	41.5	117.01	25%	11.07	0.7166	1	10.89	11.12%

*Specimens SA0, SA-H20-A, and SA-C15-A of group SA are the onlyspecimens in the research program which experienced combined punching-flexural failure

Fig. 9 Load–deflection curves of the control specimens SA0 and SB0, identical except for the slab thickness and hence the slab-to-depth ratio.

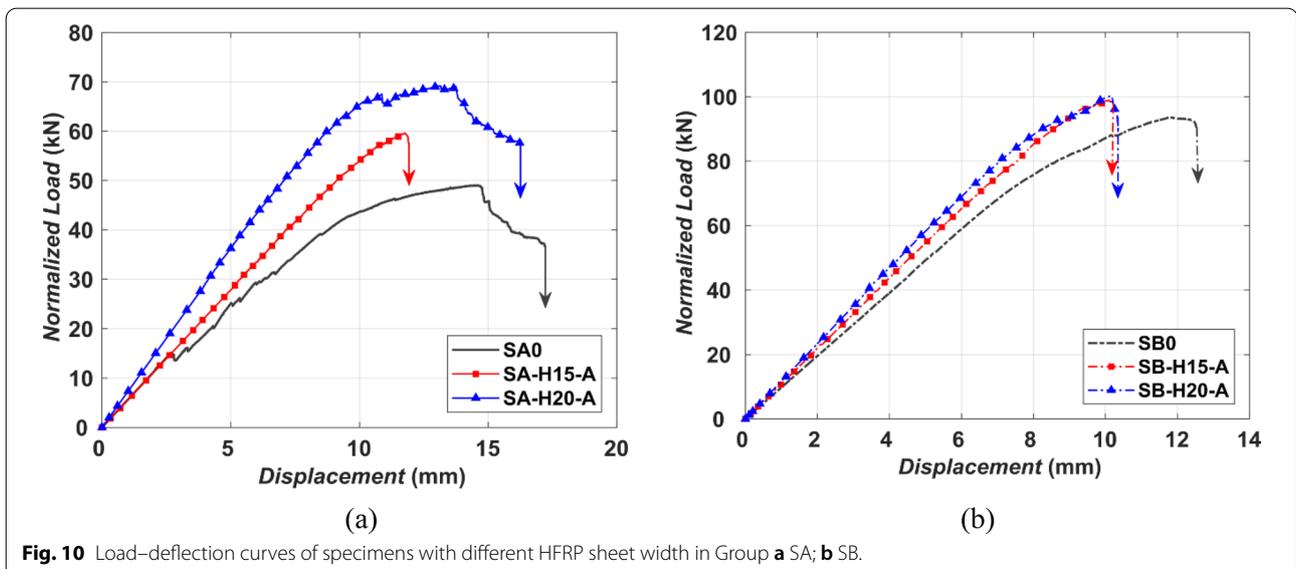### 5.2.2 Influence of the Span-to-Depth Ratio

As shown in Table 4, the increase in slab thickness from 55 (Group SA) to 75 mm (Group SB) and hence the reduction in the span to depth ratio from 25 to 18, led to a significant increase in the ultimate load capacity and the initial load–deflection stiffness of the specimens. Fig. 9 shows comparison between load–deflection responses of the control un-strengthened specimens with different slab thicknesses SA0 and SB0. The increase in ultimate load capacity of specimen SB0 relative to specimen SA0 was 91%. Moreover, the increase in fracture energy of SB0 relative to SA0 is not due to the more ductile post-ultimate load–deflection history, which does

not exist due to the pure punching failure of specimens of SB0, but rather due to the much greater ultimate load.

5.2.3 Influence of the Width of HFRP Sheets

Fig. 10a shows the normalized load–deflection curves for three specimens in Group SA confined with adjacent HFRP sheets of different widths (0, 15 and 20 cm). Specimen SA-H15-A had a pure punching shear failure, whereas the other two specimens had combined punching-flexural failure. Referring to Fig. 10a and the results listed in Table 4, specimens with 15 and 20 cm wide HFRP sheets had increases of 21.63% and 41.14% in the capacity values relative to the control specimen SA0. This could be attributed to the fact that most of the tensile cracks were covered by the increased width of the HFRP sheets. In addition, the 20 cm HFRP sheets presence increased the fracture energy relative to SA0. The 15 cm HFRP sheet specimen SA-H15-A had lower fracture energy than SA0, because it experienced pure punching shear failure compared to the combined punching-flexural failure of SA. Moreover, the strengthened specimens SA-H15-A, and SA-H20-A displayed higher initial load–deflection stiffness as compared to the control specimen SA0; the increases were 20.9% and 56.8%, respectively.

Fig. 10b shows the normalized load–deflection curves for the specimens SB0, SB-H15-A, and SB-H20-A. Strengthened specimens by adjacent HFRP sheets, SB-H15-A and SB-H20-A, displayed higher ultimate punching shear capacity and initial stiffness than the un-strengthened specimen SB0 (refer to Fig. 10b and Table 4). Relative to SB0, the increases in ultimate strength were 5.7% for specimen SB-H15-A

(a)

(b)

Fig. 10 Load–deflection curves of specimens with different HFRP sheet width in Group **a** SA; **b** SB.

and 7.25% for specimen SB-H20-A, and the increases in initial stiffness were 9.5% and 19.25%, respectively. The increase of the sheet width from 15 to 20 cm led to more significant increase in ultimate punching shear strength of the specimens in Group SA as compared to Group SB.

5.2.4 Influence of Location of HFRP Sheets

Considering the effect of the location of HFRP sheets relative to the column face in Group SA, Fig. 11a displays the normalized load–deflection responses of specimens SA0, SA-H15-A, and SA-H15-O. The HFRP sheet's location did not affect the mode of failure of the strengthened slabs, where both specimens SA-H15-A and SA-H15-O experienced pure punching failure. As shown in Fig. 11a and Table 4, the offset location of the strengthening HFRP sheets at 1.5d from the face of the column led to higher increase in ultimate punching shear strength relative to the control specimen SA0 as compared to the adjacent location (28.44% compared to 21.63%). This can be explained by the fact that the sheets in the offset position covered the generated major cracks, leading to an increase in the punching shear capacity. Moreover, the sheets offset location had a positive impact on the initial stiffness of the load deflection curve.

Fig. 11b shows the normalized load–deflection curves for the specimens SB0, SB-H15-A, and SB-H15-O. In general, the offset location of the HFRP sheet from the column face in Group SB produced higher ultimate punching shear capacity than the specimen with adjacent sheets (15.7% compared to 5.7%). In addition, the offset location led to increase in the initial load–deflection
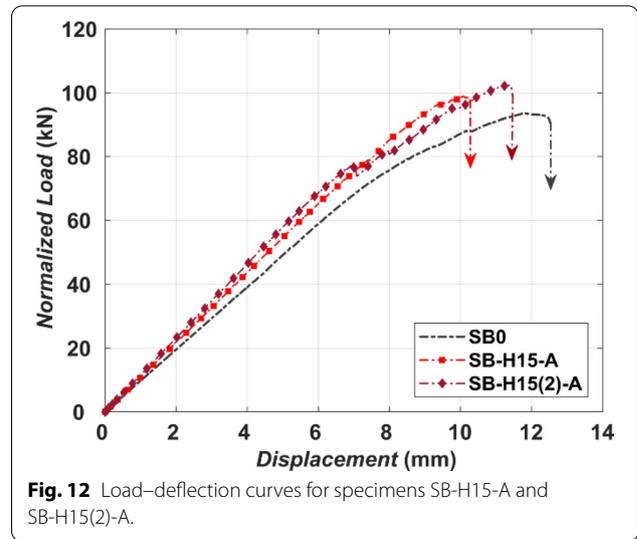

Fig. 12 Load–deflection curves for specimens SB-H15-A and SB-H15(2)-A.

stiffness. These findings are in line with the results of Group SA.

5.2.5 Influence of Number of Layers of HFRP Sheets

The effect of doubling the number of layers of the strengthening HFRP sheet was investigated in Group SB. Fig. 12 compares the normalized load–deflection curves of specimens SB-H15-A and SB–H15(2)-A. The ultimate shear capacity reached by SB-H15-A and SB-H15(2)-A were comparable: 98.9 and 102.4 kN, respectively. It can be clearly seen that both specimens displayed comparable response in terms of the mode of failure, initial stiffness, and ultimate punching shear strength. This could
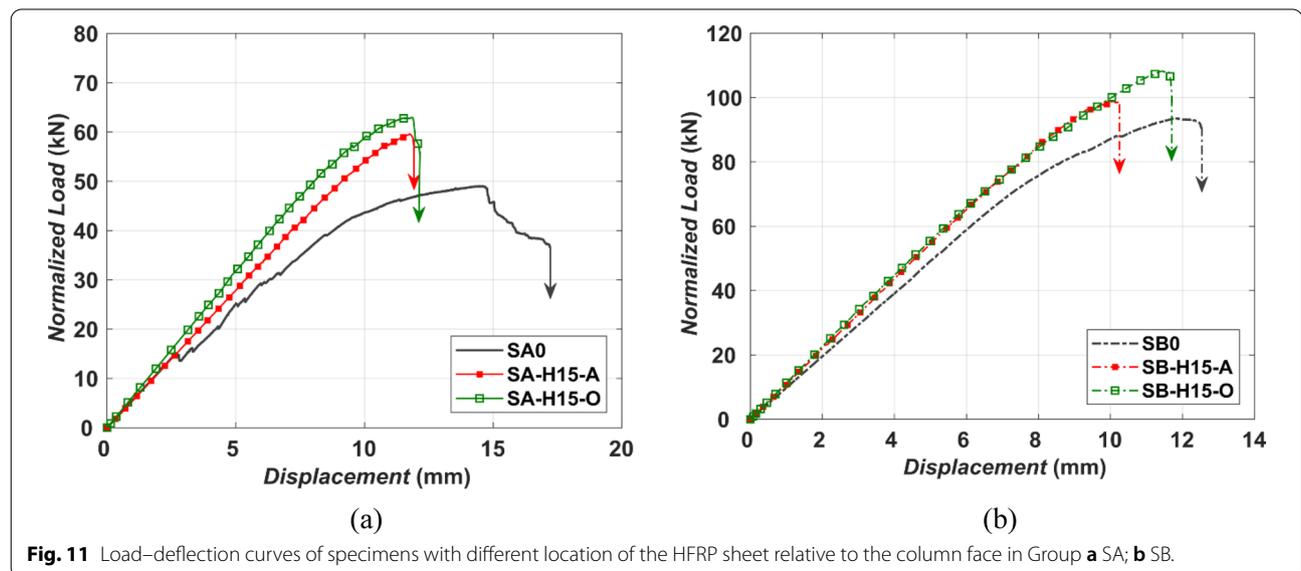

Fig. 11 Load–deflection curves of specimens with different location of the HFRP sheet relative to the column face in Group **a** SA; **b** SB.
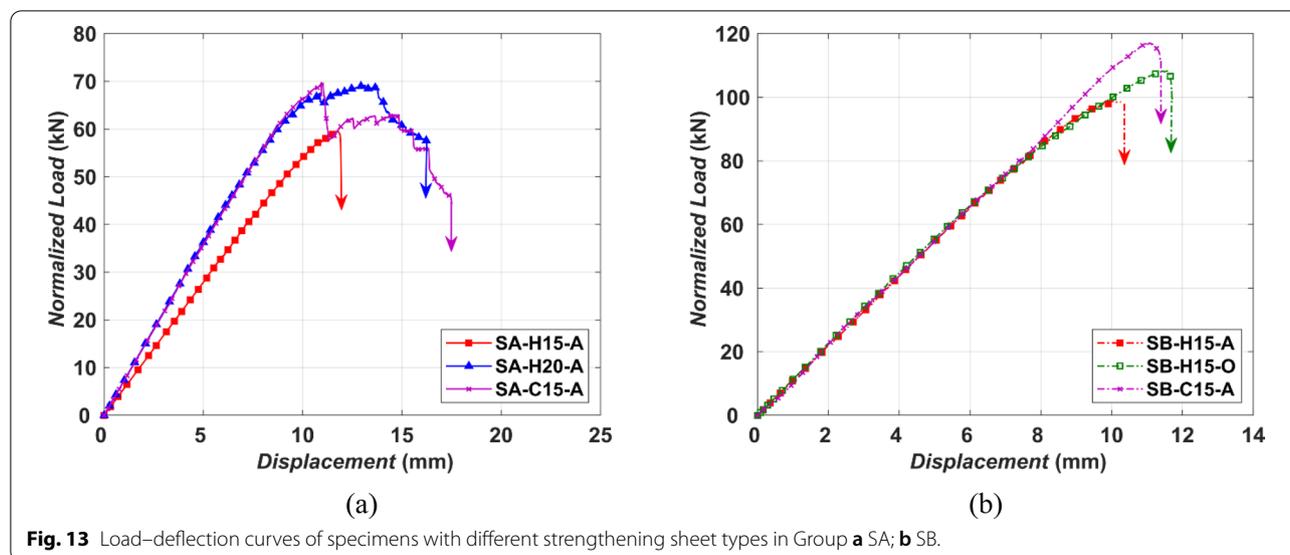
Fig. 13 Load–deflection curves of specimens with different strengthening sheet types in Group **a** SA; **b** SB.

be explained by premature rupture of the second HFRP sheet in specimen SB-H15(2)-A at a load level of 78 kN, after which the specimen continued to perform as a single layer HFRP specimen.

5.2.6 Influence of the Type of Strengthening Sheet: HFRP versus CFRP

Fig. 13a shows the load deflection response for specimens SA-H15-A, SA-C15-A, and SA-H20-A. The CFRP specimen's performance was superior in terms of increase in punching shear capacity and initial load–deflection stiffness as compared to the HFRP specimen (refer to Fig. 13a and Table 4). The increases in ultimate punching shear strength and stiffness, relative to the control specimen SA0, were 42.24% and 54.8% for specimen SA-C15-A and 21.63% and 20.9% for specimen SA-H15-A. This is supposedly due to the higher tensile strength and stiffness of the CFRP material as compared with HFRP. However, when the natural HFRP sheet width increased from 15 to 20 cm, specimen SA-H20-A exhibited approximately the same performance in load capacity and initial stiffness as specimen SA-C15-A, despite the difference in mechanical properties of the two materials. The increases in the ultimate load capacity relative to the control specimen SA0 were 41.14 and 42.24% for specimens SA-H20-A and SA-C15-A, respectively. This finding could be interpreted by the fact that the adjacent 20 cm HFRP sheets covered most of the tensile cracks in the tested specimen. It is important to note that both specimens SA-H20-A and SA-C15-A experienced combined punching-flexural failure.

Fig. 13b presents the load–deflection histories of the tested specimens SB-H15-A, SB-H15-O, and SB-C15-A. All specimens exhibited similar initial load–deflection stiffness response. As indicated in Group SA, the significant difference between these two materials mechanical properties contributed to the inferior ultimate load performance of the HFRP specimen SB-H15-A relative to the specimen SB-C15-A (117 kN compared to 98.9 kN as shown in Table 4). This difference decreased when the HFRP sheets were placed 1.5d offset from the column face in specimen SB-H15-O (117 kN compared to 108.25 kN).

5.2.7 HFRP and CFRP Strains

Fig. 14 shows typical normalized load versus strain curves recorded in the confining CFRP and HFRP sheets of the tested specimens; the relationship is found to be bilinear, similar to what was previously observed in the load–deflection response. Before cracking of the slab specimen, a very small strain was recorded in the strengthening sheets (HFRP or CFRP) and the slope of the curve is relatively steep. However, as the applied load was increased, the concrete slab's tensile cracks started to appear, leading to decrease in slope of the curve and approximately linear behavior in the load-strain response of the sheets until failure of the specimen occurred. The maximum strains measured at the center of the HFRP and CFRP confining sheets of all tested specimens are summarized in Table 5. The bottom sheets referred to in Table 5 are the ones that were bonded first to the specimen and are directly attached to the concrete surface, and the top sheets are the ones which were placed in the
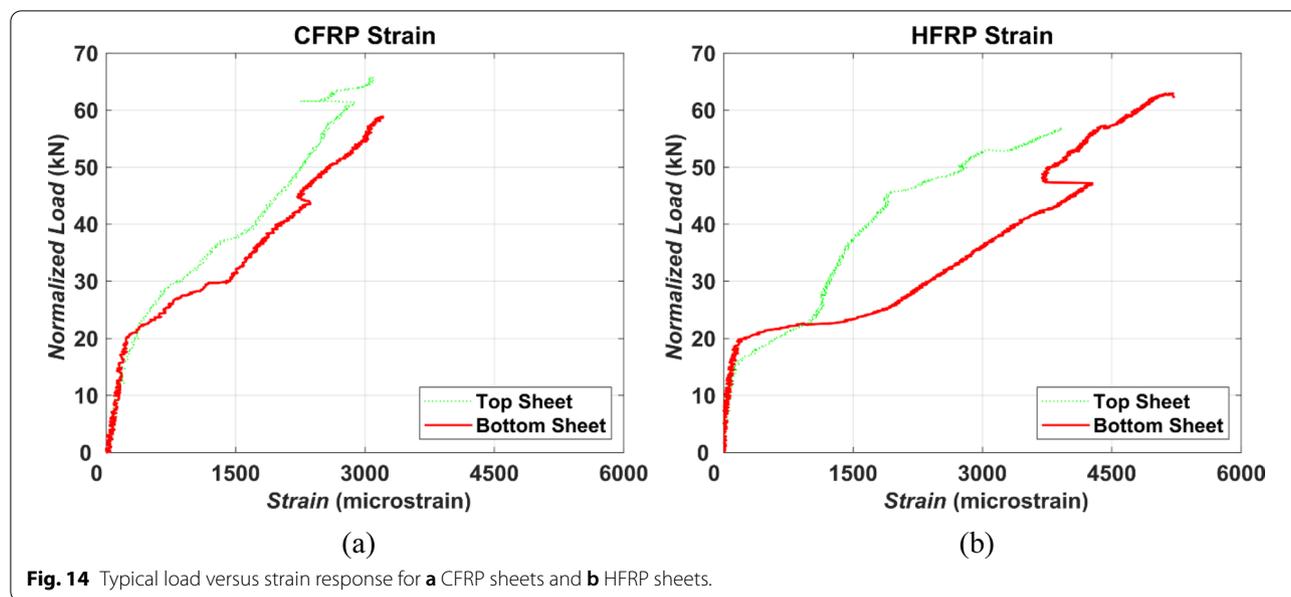
Fig. 14 Typical load versus strain response for **a** CFRP sheets and **b** HFRP sheets.

Table 5 Measured (HFRP-CFRP) ultimate strains.

Specimen designation	Ultimate strain (µɛ)	
	Location of strain gauge	
	Bottom sheets	**Top sheets**
SA-H15-A	3,660.8	–
SA-H15-O	3,928	5,223.4
SA-H20-A	–	5,773.2
SA-C15-A	3,219.8	3,105.1
SB-H15-A	6,517.5	4,184.2
SB-H15-O	9,750.8	2,572.5
SB-H20-A	9,137.4	–
SB-H15(2)-A	4,226.2	4,858.1
SB-C15-A	6,767.1	5,223.8

normal direction above the bottom ones. In general, the strains recorded in specimens with slab thickness of 75 mm (Group SB) are higher than those recorded in slabs with slab thickness 55 mm (Group SA); this can be explained by the fact that the larger effective depth in Group SB allowed larger stresses to act upon the strengthening sheets. Referring to Table 5, the offset sheets had higher strains than the adjacent ones; this could be attributed to the fact that the offset sheet covered most of generated major cracks. Strain in the bottom strip of connection SB-H15(2)-A was the smallest strain as compared to all the other bottom strips in Group SB, because the stress in this specimen was distributed between the two HFRP sheets.

6 Numerical and Analytical Investigations

A numerical model was calibrated to simulate the behavior of the tested specimens using the finite-element approach with the ABAQUS software (Smith, 2009). Analytical modeling was also conducted by adopting a model developed by Harajli and Soudki (2003) that determines the punching shear strength of the strengthened slab-column connections.

6.1 Numerical Modeling

A numerical procedure was conducted to model and determine numerically the performance of the three slab-column specimens of Group SB: the control unstrengthened specimen SB0, specimen SB-H15-A representing specimens strengthened by HFRP, and specimen SB-C15-A representing specimens strengthened by CFRP.

6.1.1 Finite-Element Model Construction

A nonlinear 3D finite-element model (FEM) model was prepared, using the finite-element software ABAQUS, to simulate the performance of interior concrete slab-column connections. The model consists of four main parts: concrete slab, reinforcement steel, strengthening sheets, and support system. The slab was considered a deformable solid part simulated with an eight-node brick element with reduced integration (C3D8R). The reinforcement was modeled as a wire deformable element 2-node linear 2-D truss (T3D2) embedded in the concrete element assuming a perfect bond between two materials (Silva et al., 2019). A mesh size of 5 mm was

Table 6 Material properties of adhesive.

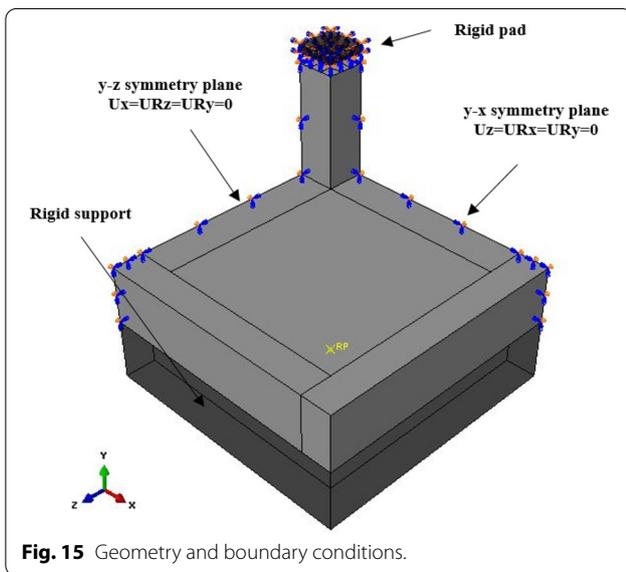| Parameters		Sikadur 330
Elastic modulus of adhesive (GPa)	E_a	4.82
Nominal stress normal mode only (MPa)	t_n	31.28
Nominal stress shear directions (MPa)	t_s, t_t	31.28
Elastic stiffness of the adhesive in normal direction (N/mm^3)	K_{nn}	4.72×10^{13}
Elastic stiffness of the adhesive in shear directions (N/mm^3)	K_{ss}, K_{tt}	2.36×10^{13}
Fracture energy of the adhesive in normal direction (N/mm)	G_n	1
Fracture energy of the adhesive in shear directions (N/mm)	G_s, G_t	1.25

Fig. 15 Geometry and boundary conditions.

Table 7 Damage properties of concrete.

Dilation Angle (φ)	Eccentricity (ε)	Stress parameters (F_{b0}/f_{c0})	Shape factor (Kc)	Viscosity Parameter (μ)
36	0.1	1.16	0.667	0.0001 (calibrated)

Table 8 Steel reinforcement properties.

Parameter	Value
Modulus of elasticity (GPa)	210
Poison's ratio	0.3
Yield stress (MPa)	570
Failure stress (MPa)	640

introduced for the steel bars. The strengthening sheets were modeled using a 4-node doubly curved shell element (SAR) with mesh size equal to 10 mm and bonded to the concrete surface by cohesive interaction. The adhesive material properties used to assign the cohesive interaction are listed in Table 6 as reported by Kabir et al. (2016). A rigid body constraint was assigned to the support system to reduce computational time and neglect its stress. The interaction between the support and concrete is normal hard contact and tangential contact with a 0.2 friction coefficient (Rasoul et al., 2019).

Due to the specimen symmetry, only one-quarter of the specimen was modeled with relevant boundary conditions to reduce the analysis computational time. The boundary conditions consisted of a fixed constrain, which was assigned on the reference point of the rigid support, and the symmetric planes were restrained in their perpendicular directions, as shown in Fig. 15. The connection was subjected to load through a rigid pad placed above the column stub with displacement control in ABAQUS/Standard.

The concrete damaged plasticity (CDP) approach was adopted to model the concrete material. The concrete material parameters that were used in the presented analysis are: the modulus of elasticity (28,800 MPa), Poisson's ratio ν (0.18), compressive f'c (35 MPa), and concrete tensile strength (assumed to be 3.5 MPa). Moreover, the concrete damaged plasticity parameters used are:

- Dilation angle (φ): According to Genikomsou (2015), the effective range of the dilation angle is between 30° and 40°; a value of 36° was used in the analysis.
- Shape factor coefficient (**Kc**): For normal concrete strength, this factor ranges between 0.64 and 0.8; a value of 0.67 was used (Smith, 2009).
- Eccentricity (ε): A default value of 0.1 was taken for the potential flow eccentricity (Smith, 2009).
- Stress parameters (**F_{b0}/f_{c0}**): For normal strength concrete, the value ranges between 1.10 and 1.16; a value of 1.16 was used in this research (Lee & Fenves, 1998).

Table 9 Composites material properties.

Parameter	CFRP	HFRP
Tensile strength (MPa)	3500	30
Modulus of elasticity (MPa)	230,000	3700
Poison's ratio	0.25	0.3
Thickness (mm)	0.13	1.2

Fig. 16 Experimental versus numerical results for different mesh sizes.

Fig. 17 Mesh scheme and springs representation.

Fig. 18 Load–displacement response for the numerical model with different values of (K).

- The viscosity parameter (**μ**): This parameter was determined by conducting a sensitive analysis (0.0001).

The damage properties are presented in Table 7. The steel's behavior in the numerical model was introduced as elastic–plastic material; the reinforced steel bars properties are listed in Table 8. The behavior of the composite sheets was modeled as elastic lamina with fail stress. In general, two types of composites were used to reinforce the connections: HFRP and CFRP. The mechanical properties for composite materials used in the numerical model are shown in Table 9.

6.1.2 Calibration of the Model
A mesh sensitivity analysis was conducted to determine the best mesh size that provides the most comparable results in term of ultimate load. Three mesh sizes (15 mm, 20 mm, and 25 mm) were adopted in this investigation. The selected values should be larger than the aggregate size (10 mm) but not too large leading to a coarse mesh (Genikomsou, 2015). The mesh size of 15 mm divided the slab thickness into five elements, while the mesh sizes of 20 and 25 mm, divided it into 4 and 3 elements, respectively. Fig. 16 presents the results of ultimate load against different mesh sizes. The results are mesh dependent, where the coarse (25 mm) and the fine (15 mm) mesh
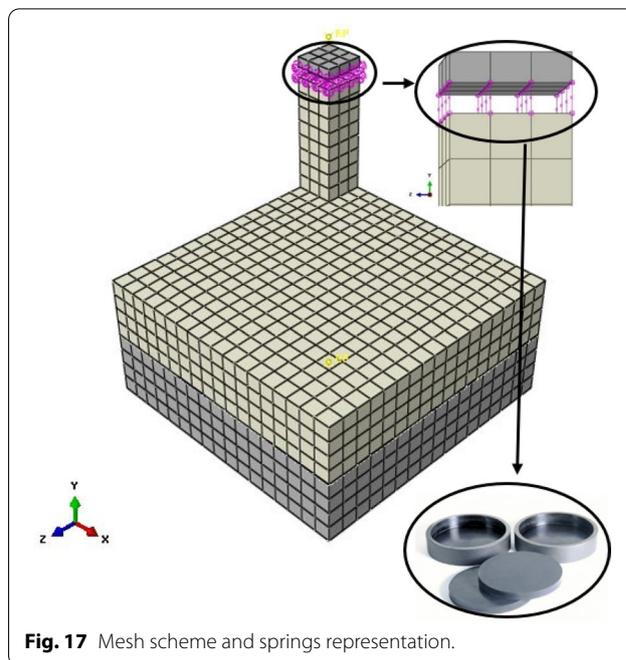
sizes provided load values different from the experimental results. However, mesh size 20 mm showed an excellent agreement with the experimental test data, as already observed in other studies (Genikomsou & Polak, 2016). Therefore, mesh size 20 mm was considered in all subsequent simulations.

During the lab testing, a steel cap with rubber was used on the top of the column stub to ensure the column would not fail before the slab. However, due to the fact the LVDT's were placed above this cap, the load–displacement reading is highly affected by the existence of

rubber material. To consider the effect of the rubber pad on the load–displacement response, a square rigid part with dimensions $50 \times 50 \times 12.7$ mm was introduced to the model and then connected to the top of the column stub by 16 springs (4×4) with an initial length $Lo = 12.7$ mm spaced at 12.5 mm (Fig. 17). The current FEM was re-executed several trials to capture the most suitable stiffness property (K) of the springs. Fig. 18 shows the load–deflection curve for some of these trials. The load–deflection response of the model with a $K = 190$ N/mm showed good agreement with that of the experimental one compared to other stiffnesses.

6.1.3 FEM Results and Discussion

The numerical results are studied by comparing the simulated connection's behavior with the experimental results in terms of cracking pattern, load–deflection response, ultimate load, and ultimate displacement. Fig. 19 displays the deflection of the connection provided by numerical analysis. The maximum deflection is detected at the center of the connection. A slight uplift of corners was noted during testing; the numerical model validated this observation. A positive contours color was observed at the edges of the connection representing the corners uplifting.

In the numerical analysis, plastic strain (PE) was used to present the connection cracking pattern. The experimental and numerical crack patterns on the tension surface of the connections were very similar at ultimate failure load. The plastic strain contour and the experimental propagated cracks were approximately the same in the simulated connections. Therefore, the FEM can predict the development of the cracks of slab-column connection.

A comparison between the experimental and numerical results is presented in Table 10. The numerical model provided ultimate loads which are similar to the experimental results, where the relative errors between numerical and experimental results for specimens SB, SB-H15-A, and SB-C15-A are 0.39%, 0.4%, and 3.95%, respectively. The numerical values for the displacement of SB, SB-H15-A, and SB-C15-A, at ultimate load, are 11.45, 11.23, and 12.24 mm, respectively; they are comparable to the experimental results (11.77, 10.09, and 11.07 mm, respectively).

Fig. 20 compares the numerical and experimental load–deflection responses for the simulated specimens. It clearly shows that the numerical model can predict the behavior of the specimen, where pure punching shear failure is observed (which is characterized by a sharp
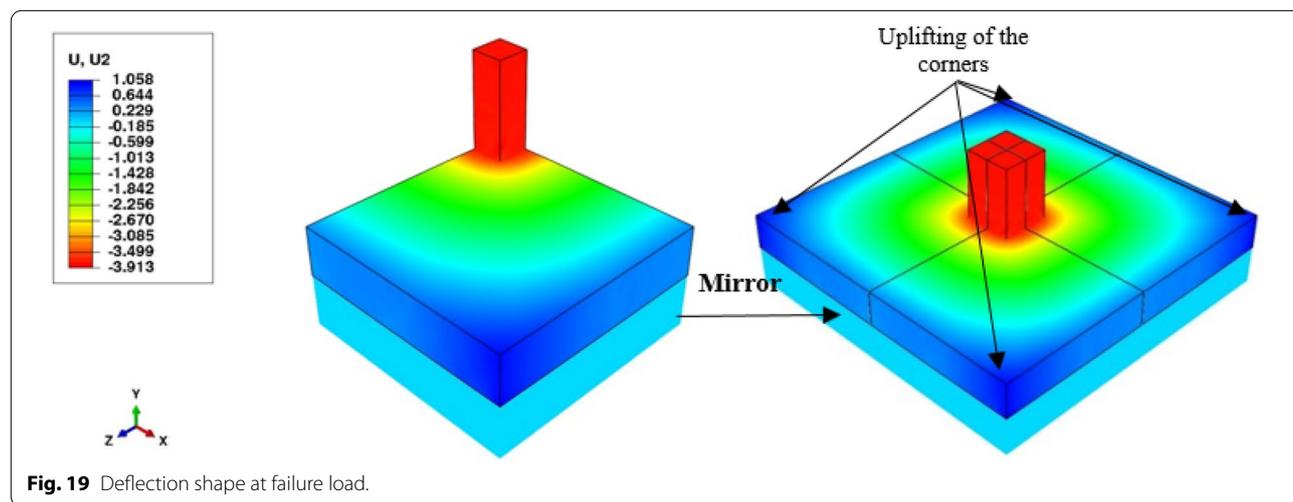

Fig. 19 Deflection shape at failure load.

Table 10 Comparison between experimental and numerical results.

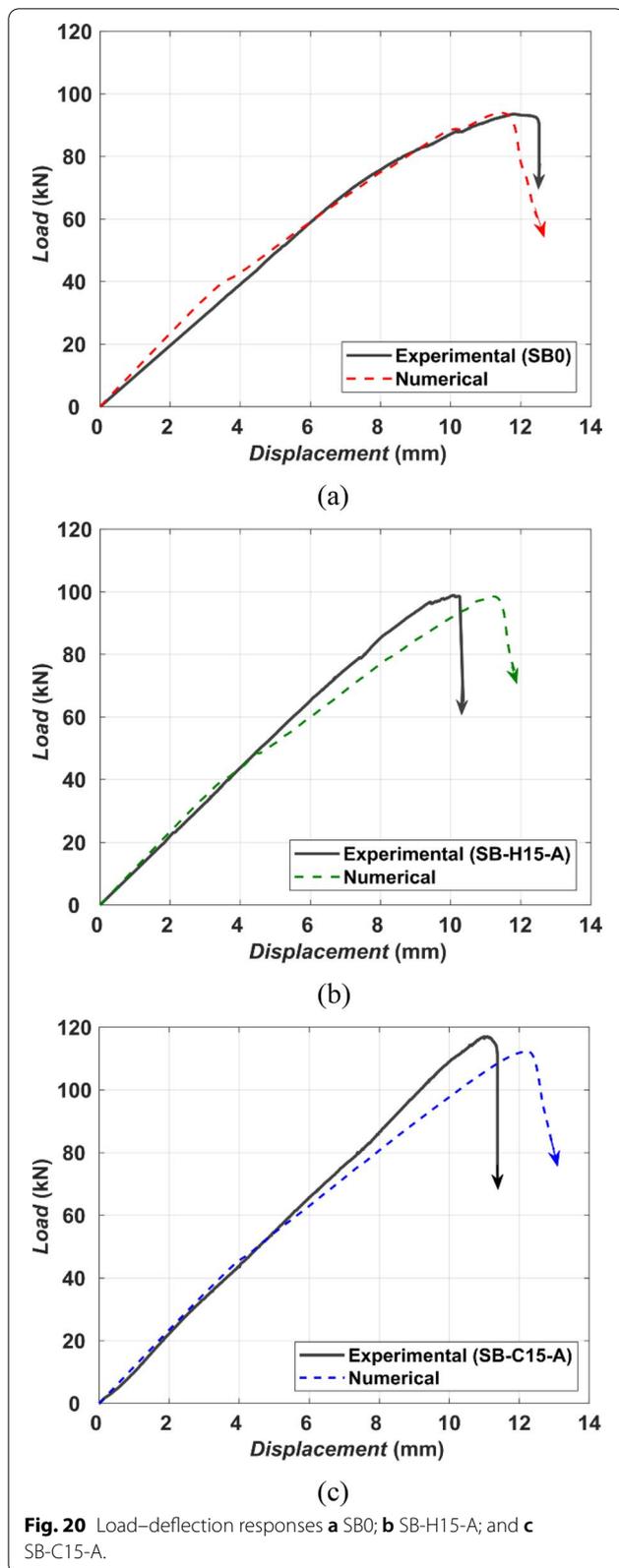| Specimen designation	Experimental results		Numerical results		P_{UFEM} / P_{Uexp}	Δ_{FEM} / Δ_{exp}
	Ultimate Load P_{Uexp} (kN)	Deflection at $P_U\Delta_{exp}$ (mm)	Ultimate Load P_{UFEM} (kN)	Deflection at $P_U\Delta_{FEM}$ (mm)		
SB0	93.57	11.77	93.93	11.45	1.004	0.973
SB-H15-A	98.9	10.09	98.5	11.23	0.996	1.113
SB-C15-A	117.02	11.07	112.4	12.24	0.961	1.106

Fig. 20 Load–deflection responses **a** SB0; **b** SB-H15-A; and **c** SB-C15-A.

drop in load) in the numerical curves as the case with the experimental results.

6.2 Analytical Modeling

The analytical model proposed by Harajli and Soudki (2003) was selected to predict the punching shear strength of strengthened connections. Harajli and Soudki suggested that the punching shear capacity of the slab is highly affected by its flexural capacity. To consider the contribution of strengthening sheets on the flexural capacity of the connections, the average moment capacity per unit width (m) of the strengthened slab was derived using the conventional force and moment equilibrium strain compatibility requirements across the depth of the slab section as follows:

$$
\begin{aligned}
m = {}& \rho_s f_y d^2 \left[1 - 0.59 \left(\rho_s \frac{f_y}{f'c} + \rho_f \frac{k_v f_{fu}^{h/d}}{f'c} \right) \right] \\
& + \rho_f k_v f_{fu} h^2 \left[1 - 0.59 \left(\rho_s \frac{f_y^{d/h}}{f'c} + \rho_f \frac{k_v f_{fu}}{f'c} \right) \right]
\end{aligned}
\tag{1}
$$

The reinforcement ratios of internal steel and external FRP reinforcement are given as

$$
\rho_s = \frac{As}{wd}; \ \rho_f = \frac{A_{frp}}{wh}
\tag{2}
$$

A_s is the cross-sectional area of steel used per slab panel of width w (mm^2); A_{frp} is the cross-sectional area of the FRP strips (mm^2); h is the overall height of the slab section (mm); d is the effective depth of tension steel reinforcement (mm); f_y is yield stress of reinforcing steel (MPa); f'c is the concrete compressive strength (MPa); f_{fu} is the ultimate strength of the FRP strips (MPa).

The k_v factor in Eq. (1) accounts for the possible delamination failure from the concrete (ISIS Canada, 2001), and can be calculated as follows:

$$
k_v = \frac{K_1 K_2 Le}{11,900 \varepsilon_{fu}} \leq 0.75
\tag{3}
$$

where *Le* is the length over which the bond stress is maintained (mm); it is defined as

$$
Le = \frac{25,350}{\left(t_f E_f \right)^{0.58}}
\tag{4}
$$

where t_f and E_f represent the CFRP strip thickness (mm) and modulus of elasticity (MPa), respectively. The factors, K_1 and K_2, which account for the concrete strength and wrapping scheme, are

$$K_1 = \left(\frac{f'c}{27}\right)^{\frac{2}{3}} \tag{5}$$

$$K_2 = \frac{L_f - 2Le}{L_f} \tag{6}$$

where L_f is slab length or width dimension in the direction of FRP sheets (mm). It should be noted that k_v of HFRP specimens is considered 1, because the primary reason for the failure of the sheets was tensile rapture (no delamination failure was observed).

The area of the composite sheets including the effects of strengthening configuration can be calculated by the model proposed by Sharaf et al. (2006)

$$A_f = \sum_{i=1}^{n} \frac{\eta}{\zeta} b_{fi} t_{fi} \tag{7}$$

where n is the total number of composite sheets per slab width; b_{fi} is width of composite sheet (mm); t_{fi} is thickness of composite sheet (mm); n is the factor that represents the effect of composite sheets orientation, taken as 1 for orthogonal sheets. The factor ζ accounts for the effect of composite sheets location relative to the column face and can be calculated as follows:

$$\zeta = \frac{\sum_{i=1}^{n} \frac{b_{fi}}{s_i}}{n} \tag{8}$$

where s_i is the distance from center of each composite sheet to the column face (mm).

The flexural capacity of the slab, P_{flex} (kN) can be calculated based on the yield line analysis as follows (Elstner & Hognestad, 1956):

$$P_{flex} = 8m\left(\frac{1}{1 - r/w} - 3 + 2\sqrt{2}\right) \tag{9}$$

where r is the side length of a square loaded area or width of a column (mm).

The punching shear strength, Pu (kN) of the strengthened slab is calculated according to the equation proposed by Mowrer and Vanderbilt (1967) as follows:

$$P_u = \frac{0.8(1 + d/r)bd\sqrt{f'c}}{1 + \left(0.433bd\sqrt{f'c}/P_{flex}\right)} \tag{10}$$

where b is the perimeter of the column or loaded area (mm).

Table 11 summarizes the comparison between the analytical results relative to the experimental results. It can be noted that the analytical model proposed by Harajli and Soudki (2003) provides good prediction of the punching shear capacity for the tested specimens in this study. The average ratio of the experimental punching shear strength values to the analytical predictions $P_{u\ test}/P_{u\ calc}$ is 0.991 with a standard deviation of 0.108. Whereas the ratio ($P_{u\ test}/P_{u\ calc}$) ranges between 1.011 and 1.165 for Group SA of 55 mm thick slabs, it ranges between 0.866 and 0.999 for Group SB of 75 mm thick slabs. Similar trend of this ratio was reported by Harajli and Soudki (2003) for specimens confined with CFRP sheets.

7 Conclusions

The reported research examines the applicability of using externally bonded HFRP fabric sheets as punching shear strengthening of slab-column connections. Eleven

Table 11 Comparison between experimental and analytical results.

Specimen designation	$P_{u\ test}$ (kN)	A_{frp} (mm^2)	m (kN-m/m)	P_{flex} (kN)	$P_{u\ calc}$ (kN)	$P_{u\ test}/P_{u\ calc}$
SA-H15-A	59.6	180	7.524	60.43	58.97	1.011
SA-H15-O	62.9	313.2	7.807	62.7	59.8	1.052
SA-H20-A	69.16	240	7.65	61.45	59.35	1.165
SA-C15-A	69.7	19.5	8.7	69.88	62.2	1.121
SB-H15-A	98.9	180	17	136.57	114.247	0.866
SB-H15-O	108.25	378	17.57	141.08	115.32	0.939
SB-H15(2)-A	102.43	360	17.52	140.67	115.22	0.889
SB-H20-A	100.35	240	17.176	137.94	114.58	0.876
SB-C15-A	117.01	19.5	18.58	149.22	117.14	0.999
Average						**0.991**
Standard deviation						**0.108**
Coefficient of variation (%)						**10.9**

small-scale interior RC slab-column connections were tested. The research focused on five main parameters that may affect the behavior of strengthened slab-column connections. These parameters were slab thickness, HFRP sheet width, location of HFRP sheet relative to the column face, number of layers of HFRP sheets, and strengthening sheet type (CFRP or HFRP). A numerical model was calibrated to simulate the behavior of tested specimens, and an analytical model was used to predict their ultimate load capacity.

Based on the test results, the following observations and conclusions could be made:

1. Increasing the slab thickness from 55 to 75 mm and thus reducing the span-to-depth ratio from 25 to 18, led to a remarkable increase in the load–deflection initial stiffness and the ultimate load capacity.
2. The structural behavior of the tested connections was considerably improved using externally bonded HFRP sheets based on the slab thickness, sheet width, and sheet configuration. The improvement in the ultimate shear capacity ranged between 5.7% and 41.14%, while the increase in stiffness reached up to 56.8% relative to the control un-strengthened specimen.
3. In general, the offset location of the strengthening sheets from the column face produced higher increase in the shear capacity than the adjacent to the column face location.
4. Adding more layers of HFRP sheets did not improve the structural behavior of the tested connections due to the premature rupture failure of the second HFRP sheet.
5. Although the performance of specimens strengthened by synthetic CFRP sheets was superior to the natural HFRP confined specimen due to the big difference in the two materials' mechanical properties, this improved performance could be reached by the natural HFRP sheets when they were applied in larger width or different configurations.
6. A numerical model was prepared using the finite-element method, and was calibrated to simulate the tested specimens' performance. The numerical model accuracy was validated against three tested specimens. The numerical predictions showed good agreement with experimental results in terms of cracking pattern, load–deflection response, and ultimate load and its corresponding displacement.
7. The analytical investigation was conducted by adopting a model proposed by Harajli and Soudki (2003) to predict the punching shear capacity for strengthened specimens. Comparing the model prediction with the experimental results showed that the available

model provides accurate predictions for the tested specimens punching shear capacity.

Author Contributions

Both authors contributed to the research reported in the paper. Both authors read and approved the finalmanuscript.

Authors' information

Loai Al-Mawed is a graduate Student in the CEE Department at the American University of Beirut.
Bilal Hamad is a Professor in the CEE Department at the American University of Beirut.

Availability of Data and Materials

Manuscript does not include any individual person's data.

Declarations

Competing Interests

The authors declare that they have no known competing financial interests or personal relationships that could have appeared to influence the work reported in this paper.

References

ASTM C39. (2021). Standard test method for compressive strength of cylindrical concrete specimens. *ASTM International*, West Conshohocken, PA. https://doi.org/10.1520/C0039.

ASTM C494. (2020). Standard Specification for Chemical Admixtures for Concrete. *ASTM International,* West Conshohocken, PA. https://doi.org/10.1520/C0494.

ASTM D3822/D3822M-14. (2020). Standard test method for tensile properties of single textile fibres. *ASTM International,* West Conshohocken, PA. https://doi.org/10.1520/D3822.

Awwad, E., Hamad, B., Mabsout, M., & Khatib, H. (2014). Structural behavior of simply supported beams cast with hemp-reinforced concrete. *ACI Structural Journal, 111*(6), 1307–1316. https://doi.org/10.14359/51687032

Chen, C. C., & Chen, S. L. (2020). Strengthening of reinforced concrete slab-column connections with carbon fiber reinforced polymer laminates. *Applied Sciences (switzerland), 10*, 1. https://doi.org/10.3390/app10010265

Chen, C.C. & Li, C.Y. (2005). Punching shear strength of reinforced concrete slabs strengthened with glass fiberreinforcedpolymer laminates. *ACI Structural Journal, 102* (4), 535–542.

Elstner, R. C., & Hognestad, E. (1956). Shearing strength of reinforced concrete slabs. *ACI Journal Proceedings, 53*(7), 29–58. https://doi.org/10.14359/11501

Genikomsou, A.S. (2015). Nonlinear finite element analysis of punching shear of reinforced concrete slabs supported on rectangular columns. *PhD Thesis*, University of Waterloo. Ontario, Canada.

Genikomsou, A. S., & Polak, M. A. (2016). Finite-element analysis of reinforced concrete slabs with punching shear reinforcement. *Journal of Structural Engineering, 142*(12), 04016129. https://doi.org/10.1061/(asce)st.1943-541x.0001603

Ghalieh, L., Awwad, E., Saad, G., Khatib, H., & Mabsout, M. (2017). Concrete columns wrapped with hemp fiber reinforced polymer - An experimental study. *Procedia Engineering, 200*(December), 440–447. https://doi.org/10.1016/j.proeng.2017.07.062

Harajli, M. H., & Soudki, K. A. (2003). Shear strengthening of interior slab–column connections using carbon fiber-reinforced polymer sheets. *Journal of Composites for Construction, 7*(2), 145–153. https://doi.org/10.1061/(asce)1090-0268(2003)7:2(145)

Harajli, M. H., Soudki, K. A., & Kudsi, T. (2006). Strengthening of interior slab–column connections using a combination of FRP sheets and steel bolts. *Journal of Composites for Construction, 10*(5), 399–409. https://doi.org/10.1061/(asce)1090-0268(2006)10:5(399)

Kabir, M. H., Fawzia, S., Chan, T. H. T., & Badawi, M. (2016). Numerical studies on CFRP strengthened steel circular members under marine environment. *Materials and Structures/Materiaux Et Constructions, 49*(10), 4201–4216. https://doi.org/10.1617/s11527-015-0781-5

King, S., & Delatte, N. J. (2004). Collapse of 2000 Commonwealth Avenue: Punching shear case study. *Journal of Performance of Constructed Facilities, 18*(1), 54–61. https://doi.org/10.1061/(asce)0887-3828(2004)18:1(54)

Lee, J., & Fenves, G. L. (1998). Plastic-damage model for cyclic loading of concrete structures. *Journal of Engineering Mechanics, 124*(8), 892–900.

Lubliner, J., Oliver, J., Oller, S., & Onate, E. (1989). A Plastic-Damage Model. *International Journal of Solids and Structures, 25*(3), 299–326.

Mirzaei,Y., & Sasani, M. (2011). Punching shear failure in progressive collapse analysis. *Structures Congress 2011*, Las Vegas, Nevada. https://doi.org/10.1061/41171(401)255.

Rahman Khan, Md. M., Chen, Y., Belsham, T., Laguë, C., Landry, H., Peng, Q., & Zhong, W. (2011). Fineness and tensile properties of hemp (*Cannabis Sativa* L.) fibres. *Biosystems Engineering, 108*(1), 9–17. https://doi.org/10.1016/j.biosystemseng.2010.10.004

Rasoul, A., Zainab, M. R., Ali, H. M., & Taher, M. (2019). Accuracy of concrete strength prediction behavior in simulating punching shear behavior of flat slab using finite element approach in Abaqus. *Periodicals of Engineering and Natural Sciences, 7*(4), 1933–1949. https://doi.org/10.21533/pen.v7i4.943

Sharaf, M. H., Soudki, K. A., & Van Dusen, M. (2006). CFRP strengthening for punching shear of interior slab–column connections. *Journal of Composites for Construction, 10*(5), 410–418. https://doi.org/10.1061/(asce)1090-0268(2006)10:5(410)

Sikadur®-330 (2019). *Sikadur®-330 Product Data Sheet: 2-Component epoxy impregnation resin.* https://usa.sika.com/.

SikaWrap®-230 C. (2017). *SikaWrap®-230 C Product Data Sheet: Woven unidirectional carbon fibre fabric, designed for structural strengthening applications as part of the sika® strengthening system.* https://egy.sika.com/.

Silva, M. A. L., Gamage, J. C. P. H., & Fawzia, S. (2019). Performance of slab-column connections of flat slabs strengthened with carbon fiber reinforced polymers. *Case Studies in Construction Materials, 11*, e00275. https://doi.org/10.1016/j.cscm.2019.e00275

Siriluk, S., Hussin, Q., Rattanapitikorn, W., & Pimanmas, A. (2018). Behaviours of RC deep beams strengthened in shear using hemp fiber reinforced polymer composites. *Journal of GEOMATE, 15*(47), 89–94. https://doi.org/10.21660/2018.47.STR167

Smith, M. (2009). *ABAQUS/Standard User's Manual, Version 6.9.* Dassault Systèmes Simulia Corp, Providence, RI.

Soudki, K. A., El-Sayed, A. K., & Vanzwol, T. (2012). Strengthening of concrete slab-column connections using cfrp strips. *Journal of King Saud University - Engineering Sciences, 24*(1), 25–33. https://doi.org/10.1016/j.jksues.2011.07.001

Yinh, S., Hussain, Q., Rattanapitikon, W., & Pimanmas, A. (2016). Flexural behavior of reinforced-concrete (RC) beams strengthened with hemp fiber-reinforced polymer (FRP) composites. *Materials Science Forum, 860*, 156–159. https://doi.org/10.4028/www.scientific.net/MSF.860.156

Publisher's Note